2011 American Control Conference
on O'Farrell Street, San Francisco, CA, USA
June 29 - July 01, 2011

Target Tracking Strategies for a Nonlinear, Flexible Aircraft-Inspired Model

Animesh Chakravarthy, Katie A. Evans, Johnny Evers, and Lisa M. Kuhn

Abstract— **Aeroelastic wing micro aerial vehicle (MAV) concepts are being explored for military and civilian applications. However, on the whole, the issues of control of MAVs are largely unexplored. The authors seek to employ distributed parameter modeling and control theory in an effort to achieve agile flight potential of flexible, morphable wing MAV airframes. In this work, two Euler-Bernoulli beams connected to a rigid mass are used to model the heave dynamics of an aeroelastic wing MAV. A nonlinear aerodynamic lift force acts upon this multiple component structure. The focus of this paper is an effort to employ tools from linear distributed parameter control theory to gain insight into feasibly obtained wing shape, as a bridge to examining optimal wing morphing trajectories for achieving agile flight.**

I. INTRODUCTION

Considerable work is currently underway to investigate the aerodynamics, structural dynamics, flight mechanics, and control associated with bio-inspired flight (see, for example, [1], [2], [3], [4], [5]). Consequently, aeroelastic wing micro aerial vehicle (MAV) concepts are being explored for military and civilian applications. It is a conjecture of the United States Air Force that the flexibility of aeroelastic wings can be exploited to achieve greater advances in autonomous MAV flight. As such, efforts are underway (see, for example, [6], [7], [8], [9]) to lay the foundation required to eventually construct high fidelity dynamics models of MAVs, which do not currently exist, though key features of such models are emerging. However, on the whole, the issues of control of agile aeroelastic wing MAVs are largely unexplored. It is our goal to use distributed parameter modeling in the context of control design, with a specific focus on the ability of the wings to morph into some desired state.

In this paper, the authors use two Euler-Bernoulli beams connected to a rigid mass in an effort to model heave dynamics of an aeroelastic wing MAV. Each beam represents a flexible wing, while the rigid mass represents the fuselage. This "beam-mass-beam" model will be referred to as the BMB model system in this paper. The authors employ Linear Quadratic Regulator (LQR) state tracking to drive wing shape to a specified morphed shape. For low angles of attack, the BMB model is nearly linear, so it is reasonable to explore the potential use of linear control strategies. Subsequently, the authors make a more realistic assumption that all states are not known for feedback and design an $\mathcal{H}^2$ extended Kalman filter, specifically, the special case of the Linear Quadratic Gaussian (LQG), observer-based tracking controller to achieve a certain morphed wing shape. A comparison of results is made for the two strategies.

The outline of the paper is as follows. Section II briefly describes some well-known distributed parameter control strategies utilized in the present work. Section III provides a description of the equations governing the partial differential equation (PDE) aircraft model. The variational form and discretization of the PDE equations are provided in Section IV. Numerical results are presented in Section V, while conclusions and directions for future work are given in Section VI.

II. DISTRIBUTED PARAMETER SYSTEM (DPS) CONTROL STRATEGIES

For low angles of attack the aerodynamic lift force included in the BMB system is nearly linear, thereby making the BMB system nearly linear. Therefore, it is reasonable to consider the extent to which linear control strategies can be effectively applied to this model. This section assumes the existence of a DPS arising from a PDE, and control approaches are described in the infinite dimensional setting; theory is in place for methods considered here to guarantee convergence of finite dimensional approximations to the PDE controller under usual assumptions (see, for example, [10], [11]).

The control objectives of interest in this paper include output tracking, specifically for the purpose of morphing each beam from equilibrium to a desired, known state. This is done as an initial step to 1) ascertain the feasibility of requiring wings of a distributed parameter MAV model of realistic material specifications to transform to a specific shape and 2) gain insight into optimal wing morphing trajectories for achieving agile flight.

The first control implementation involves a Linear Quadratic Regulator (LQR) state tracking design, where the tracking problem reduces to a disturbance-rejection problem

This work was supported by NSF EPSCoR through the Louisiana Board of Regents under Contract Number NSF(2010)-PFUND-201, the US Air Force Summer Faculty Fellowship Program, and the Air Force Research Laboratory under Contract Number FA8651-08-D-0108.

A. Chakravarthy is a joint Faculty in the Depts. of Aerospace Engineering and Electrical Engineering, Wichita State University, 1845 N. Fairmount, Wichita, KS 67260, USA animesh.chakravarthy@wichita.edu

K. Evans is with the Faculty of Mathematics and Statistics, P.O. Box 10348, Louisiana Tech University, Ruston, LA 71272, USA kevans@latech.edu

J. Evers is with the Air Force Research Laboratory, Munitions Directorate, 101 W. Eglin Blvd., Ste. 332, Eglin AFB, FL 32542 USA johnny.evers@eglin.af.mil

L. Kuhn is a Ph.D. Student of Computational Analysis and Modeling, P.O. Box 10348, Louisiana Tech University, Ruston, LA 71272, USA lmk012@latech.edu

of the form

$$\dot{x}(t) = \mathcal{A}x(t) + \mathcal{B}u(t) + w(t), \quad x(0) = x_0, \tag{1}$$

where $x(t) = x(t,\cdot) = \xi(t,\cdot) - \tilde{\xi}(t,\cdot) \in X$, a Hilbert space, $w(t)$ is represented by

$$w(t) = \mathcal{A}\tilde{\xi} - \dot{\tilde{\xi}} \neq 0, \tag{2}$$

ξ is the state of some original dynamical linear system of interest,

$$\dot{\xi}(t) = \mathcal{A}_0\xi(t) + \mathcal{B}_0u(t) + z, \quad \xi(0) = \xi_0, \tag{3}$$

$\tilde{\xi}$ is the known desired state target of (3), and z is zero-mean, Gaussian, white noise. Here, $\mathcal{A}$ is the linearized system operator defined on $\mathbf{D}(\mathcal{A}) \subseteq X$ that, by assumption, generates an exponentially stable C_0-semigroup, $\mathcal{B}$ is the control operator, and $u(t)$ is the control input, defined on a Hilbert space U, which is taken to be $\mathbb{R}^m$ in this work.

The solution to the steady state tracking problem involves solving the standard control Riccati equation

$$\mathcal{A}^*\Pi + \Pi\mathcal{A} - \Pi\mathcal{B}R^{-1}\mathcal{B}^*\Pi + Q = 0 \tag{4}$$

for Π, where $Q : X \to X$ is a state weighting operator, taken to be $\mathcal{C}^*\mathcal{C}$ in this work (see (9)) and $R : U \to U$ is a control weighting operator taken to be of the form $R = cI$, with c a scalar and I the identity operator, with both operators corresponding to the standard LQR cost function. Then the feedback control gain is defined as

$$\mathcal{K} = R^{-1}\mathcal{B}^*\Pi. \tag{5}$$

The feed forward signal u_{fw} is

$$u_{fw} = R^{-1}\mathcal{B}^*q, \tag{6}$$

where an approximation of q can be calculated by integrating backwards in time to obtain the steady state solution of

$$\dot{q}(t) = -[\mathcal{A} - \mathcal{B}R^{-1}\mathcal{B}^*\Pi]q(t), \tag{7}$$

with $q(\infty) = 0$, as stated in [12]. Then the control law for the LQR state tracking is

$$u(t) = -\mathcal{K}x(t) - u_{fw}, \tag{8}$$

which is implemented in (1).

In the second control implementation involving an $\mathcal{H}^2$, specifically a Linear Quadratic Gaussian (LQG), state tracking design, it is assumed that an estimate of the state from (1) exists, based on a measurement

$$y = \mathcal{C}x(t) + v, \tag{9}$$

where measurement $y(t) : X \to Y$, with Y a Hilbert space, is taken to be $\mathbb{R}^p$ in this work, v is zero-mean, Gaussian, white noise, uncorrelated with z in (3), and the estimate, $x_c(t) = x_c(t,\cdot) \in X$, is used in the control law (8). Again, the state from (1) is $\xi - \tilde{\xi}$. It is assumed that the desired target of the state estimate is also $\tilde{\xi}$. To provide this estimate, a compensator is used that has the form

$$\dot{x}_c(t) = \mathcal{A}_cx_c(t) + \mathcal{F}_cy(t), \quad x_c(0) = x_{c_0} \tag{10}$$

and the feedback control law is written

$$u(t) = -\mathcal{K}x_c(t) - u_{fw}, \tag{11}$$

where $\mathcal{K}$ and u_{fw} are determined from the LQR tracking solution. From standard theory, it is well-known that by solving an additional filter Riccati equation

$$\mathcal{A}P + P\mathcal{A}^* - P\mathcal{C}^*\mathcal{C}P + \mathcal{B}\mathcal{B}^* = 0, \tag{12}$$

one can obtain the operators $\mathcal{F}_c$, and $\mathcal{A}_c$ via

$$\begin{array}{rcl} \mathcal{F}_c & = & P\mathcal{C}^*, \\ \mathcal{A}_c & = & \mathcal{A} - \mathcal{B}\mathcal{K} - \mathcal{F}_c\mathcal{C}. \end{array} \tag{13}$$

Under standard assumptions of stabilizability of $(\mathcal{A},\mathcal{B})$ and detectability of $(\mathcal{A},\mathcal{C})$, there are guaranteed unique solutions Π and P to (4) and (12), respectively, such that the linear closed loop system given by

$$\begin{aligned} \frac{d}{dt}\begin{bmatrix} x(t) \\ x_c(t) \end{bmatrix} &= \begin{bmatrix} \mathcal{A} & -\mathcal{B}\mathcal{K} \\ \mathcal{F}_c\mathcal{C} & \mathcal{A}_c \end{bmatrix}\begin{bmatrix} x(t) \\ x_c(t) \end{bmatrix} \\ &\quad + \begin{bmatrix} z - u_{fw} \\ \mathcal{F}_cv \end{bmatrix} \end{aligned} \tag{14}$$

is stable.

The operators $\mathcal{K}$, $\mathcal{F}_c$, $\mathcal{A}_c$ as determined above for the linearized system, are substituted into the corresponding nonlinear system

$$\dot{x}_{n\ell}(t) = \mathcal{A}_{n\ell}x_{n\ell}(t) + \mathcal{B}u_{n\ell}(t) + \mathcal{F}_{n\ell}(x_{n\ell}(t)) + \mathcal{G} + w(t), \tag{15}$$

thus producing the nonlinear observer

$$\dot{x}_c(t) = \mathcal{A}_cx_c(t) + \mathcal{F}_cy(t) + \mathcal{F}_{n\ell}(x_c(t)), \tag{16}$$

with an appropriate initial condition. Then the nonlinear closed loop system takes on the form

$$\begin{aligned} \frac{d}{dt}\begin{bmatrix} x_{n\ell}(t) \\ x_c(t) \end{bmatrix} &= \begin{bmatrix} \mathcal{A}_{n\ell} & -\mathcal{B}\mathcal{K} \\ \mathcal{F}_c\mathcal{C} & \mathcal{A}_c \end{bmatrix}\begin{bmatrix} x_{n\ell}(t) \\ x_c(t) \end{bmatrix} \\ &\quad + \begin{bmatrix} z - u_{fw} + \mathcal{F}_{n\ell}(x_{n\ell}(t)) + \mathcal{G} \\ \mathcal{F}_cv + \mathcal{F}_{n\ell}(x_c(t)) + \mathcal{G} \end{bmatrix}. \end{aligned} \tag{17}$$

III. A FLEXIBLE WING AIRCRAFT MODEL

An aeroelastic wing MAV is modeled using two Euler-Bernoulli beams connected at a rigid mass, as shown in Figure 1. The BMB model system was originally presented in [13] with a point mass and has been modified and elaborated upon in this paper. The BMB system primarily represents the heave dynamics of a MAV, which is initially assumed to be flying with wings straight and level and in equilibrium with the lift balancing the weight. Now, if there is any perturbation in the wings' shape (caused by a sudden gust, for example), then this perturbed wing shape causes a change in the local angle of attack distribution over each wing and this in turn leads to a perturbation in the lift distribution.

Each beam is modeled with both viscous and Kelvin-Voigt damping, and it is assumed that the material and inertial properties of both beams are homogeneous, uniform, and composed of latex and carbon-graphite fiber with epoxy. Denoting the displacement (which is a combination of both

rigid body and flexible motions) of the left beam from its initial equilibrium position at time t and position s_L by $w_L(t,s_L)$ and the corresponding displacement of the right beam at time t and position s_R by $w_R(t,s_R)$, the model is described as follows:

$$\begin{aligned}&\rho A\ddot{w}_L(t,s_L)+\gamma_1\dot{w}_L(t,s_L)\\&\quad+\gamma_2 I\dot{w}_L''''(t,s_L)+EIw_L''''(t,s_L)\\&\quad=b_L(s_L)u_L(t)+\frac{m_b g}{\ell_1}-\frac{0.5\rho_a v^2 c}{\ell_1}C_\ell,\end{aligned}\tag{18}$$

for $0\le s_L\le \ell_1,\ t>0$, and

$$\begin{aligned}&\rho A\ddot{w}_R(t,s_R)+\gamma_1\dot{w}_R(t,s_R)\\&\quad+\gamma_2 I\dot{w}_R''''(t,s_R)+EIw_R''''(t,s_R)\\&\quad=b_R(s_R)u_R(t)+\frac{m_b g}{\ell_2}-\frac{0.5\rho_a v^2 c}{\ell_2}C_\ell,\end{aligned}\tag{19}$$

for $\ell_1+\ell_M\le s_R\le \ell_1+\ell_M+\ell_2$, $t>0$, and where $\dot{w}_i(t,s)=\dfrac{\partial}{\partial t}w_i(t,s)$ and $w_i'(t,s)=\dfrac{\partial}{\partial s}w_i(t,s)$ with $i=L,R$ for the left or right beam, respectively, ρ is the density of the beam material, A is the cross-sectional area of the beam, E is Young's modulus, I is the area moment of inertia of the beam, γ_1 is the coefficient of viscous damping, γ_2 is the coefficient of Kelvin-Voigt damping, g is gravity, m_b is the mass of each beam, $b_L(s)$ is the control input function for the left beam, $b_R(s)$ is the control input function for the right beam, $u_L(t)$ is the controller for the left beam, $u_R(t)$ is the controller for the right beam, ρ_a is the density of air, v is the forward vehicle velocity, c is the chord length of each wing (beam width), and C_ℓ is the aerodynamic lift coefficient.

The aerodynamic lift coefficient employed in this model is the same one derived in [14] for a fruit fly model. While it was derived for a flapping flight insect, it should be noted that its relevance also holds in this framework due to the dimensionless property of the lift coefficient and the flexibility of the wings of the fruit fly. Also, the lift coefficient model can be scaled to the the size of the MAV under consideration here by the parameters of the dynamic pressure. It should be further noted that the model is based upon data for angles of attack between -9 and 90 degrees, which is appropriate for biologically inspired MAVs since it is desired that they possess agility for performing highly complex maneuvers. For the purposes of this paper, the BMB model is not actually performing flapping motion and can be viewed as an MAV in a gliding phase of flight. The lift coefficient is given by

$$C_\ell=\left[k_1+k_2\sin\left(k_3\arctan\left(\frac{\dot{w}(t,s)+k_5}{u}\right)+k_4\right)\right],\tag{20}$$

where k_1,k_2,k_3,k_4 are the best fit parameters determined from the analysis in [14]. In order to obtain real solutions and to accommodate atmospheric conditions, it has been assumed that k_4=0, and a new parameter, k_5, has been included in the model to reflect the vertical wind velocity, thereby modeling angle of attack with the arctangent term.

The elastic equations are subject to the following boundary conditions:

$$\begin{aligned}&EIw_L''(t,0)+\gamma_2 I\dot{w}_L''(t,0)=0,\\&EIw_L'''(t,0)+\gamma_2 I\dot{w}_L'''(t,0)=0,\\&EIw_R''(t,\ell_1+\ell_M+\ell_2)+\gamma_2 I\dot{w}_R''(t,\ell_1+\ell_M+\ell_2)=0,\\&EIw_R'''(t,\ell_1+\ell_M+\ell_2)+\gamma_2 I\dot{w}_R'''(t,\ell_1+\ell_M+\ell_2)=0,\\&w_L(t,\ell_1)-w_R(t,\ell_1+\ell_M)=0,\\&w_L'(t,\ell_1)-w_R'(t,\ell_1+\ell_M)=0,\\&-EIw_L''(t,\ell_1)-\gamma_2 I\dot{w}_L''(t,\ell_1)+EIw_R''(t,\ell_1+\ell_M)\\&\quad+\gamma_2 I\dot{w}_R''(t,\ell_1+\ell_M)=I_z\ddot{w}_L'(t,\ell_1),\\&EIw_L'''(t,\ell_1)+\gamma_2 I\dot{w}_L'''(t,\ell_1)-EIw_R'''(t,\ell_1+\ell_M)\\&\quad-\gamma_2 I\dot{w}_R'''(t,\ell_1+\ell_M)=m\ddot{w}_L(t,\ell_1),\end{aligned}\tag{21}$$

where m is the mass of the rigid connection between the beams and I_z is the mass moment of inertia of the rigid mass. A graphical representation of the BMB model system can be seen in Figure 1. Since one goal of this project is to

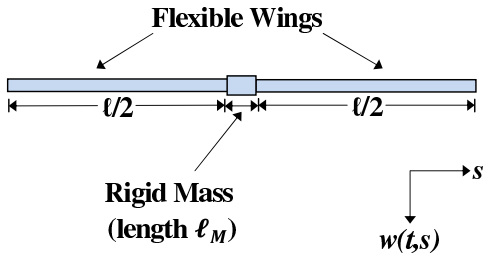

Fig. 1. MAV model system.

gain insight into optimal morphing trajectory, it is assumed that the controllers act over the entire beam structure with constant control input functions of the form

$$b_L(s_L)=b_R(s_R)=30,\tag{22}$$

for $0\le s_L\le\ell_1$ and $\ell_1+\ell_M\le s_R\le\ell_1+\ell_M+\ell_2$, and observations of the form

$$y(t)=15w(t,s),\tag{23}$$

for $0\le s_L\le\ell_1$ and $\ell_1+\ell_M\le s_R\le\ell_1+\ell_M+\ell_2$.

IV. VARIATIONAL FORM AND DISCRETIZATION OF THE BMB SYSTEM

A. Variational Form

Now consider the variational form of the BMB system in order to develop a Galerkin finite element approximation of the problem. Multiplying (18) and (19) by test functions $\phi_L(s_L)$ and $\phi_R(s_R)$, respectively, yields

$$\begin{aligned}\int_0^{\ell_1}&\left[\rho A\ddot{w}_L(t,s_L)+\gamma_1\dot{w}_L(t,s_L)+\gamma_2 I\dot{w}_L''''(t,s_L)\right.\\&\left.+EIw_L''''(t,s_L)\right]\phi_L(s_L)\,ds_L=\int_0^{\ell_1}\left[b_L(s_L)u_L(t)\right.\\&\left.+\frac{m_b g}{\ell_1}-\frac{0.5\rho_a v^2 c}{\ell_1}C_\ell\right]\phi_L(s_L)\,ds_L,\end{aligned}\tag{24}$$

and

$$\int_{\ell_1+\ell_M}^{\ell_1+\ell_M+\ell_2} \left[\rho A\ddot{w}_R(t,s_R)+\gamma_1\dot{w}_R(t,s_R)+\gamma_2 I\dot{w}_R''''(t,s_R) +EIw_R''''(t,s_R)\right]\phi_R(s_R)\ ds_R = \int_{\ell_1+\ell_M}^{\ell_1+\ell_M+\ell_2} \left[b_R(s_R)u_R(t) +\frac{m_b g}{\ell_2}-\frac{0.5\rho_a v^2 c}{\ell_2}C_\ell\right]\phi_R(s_R)\ ds_R. \tag{25}$$

Next (24) and (25) are integrated by parts, resulting equations are summed, and prescribed boundary conditions from (21) are applied. The result is a desired solution $[w_L(t,s_L),\ w_R(t,s_R)]^T \in V \subseteq S = H^2[0,\ell_1]\times H^2[\ell_1+\ell_M,\ell_1+\ell_M+\ell_2]$ such that

$$\begin{aligned}
&\int_0^{\ell_1}\left[\rho A\ddot{w}_L(t,s_L)\phi_L(s_L)+\gamma_1\dot{w}_L(t,s_L)\phi_L(s_L)\right.\\
&\left.+\gamma_2 I\dot{w}_L''(t,s_L)\phi_L''(s_L)+EIw_L''(t,s_L)\phi_L''(s_L)\right]\ ds_L\\
&+\int_{\ell_1+\ell_M}^{\ell_1+\ell_M+\ell_2}\left[\rho A\ddot{w}_R(t,s_R)\phi_R(s_R)+\gamma_1\dot{w}_R(t,s_R)\phi_R(s_R)\right.\\
&\left.+\gamma_2 I\dot{w}_R''(t,s_R)\phi_R''(s_R)+EIw_R''(t,s_R)\phi_R''(s_R)\right]\ ds_R\\
&+m\ddot{w}_L(t,\ell_1)\phi_L(\ell_1)+I_z\ddot{w}'(t,\ell_1)\phi_L'(\ell_1)\\
&=\int_0^{\ell_1}\left[b_L(s_L)u_L(t)+\frac{m_b g}{\ell_1}-\frac{0.5\rho_a v^2 c}{\ell_1}C_\ell\right]\phi_L(s_L)\ ds_L\\
&+\int_{\ell_1+\ell_M}^{\ell_1+\ell_M+\ell_2}\left[b_R(s_R)u_R(t)+\frac{m_b g}{\ell_2}-\frac{0.5\rho_a v^2 c}{\ell_2}C_\ell\right]\phi_R(s_R)\ ds_R
\end{aligned} \tag{26}$$

for all $[\phi_L(s_L),\ \phi_R(s_R)]^T \in V = \{[\phi_L(\cdot),\ \phi_R(\cdot)]^T \in S : \phi_L(\ell_1) = \phi_R(\ell_1+\ell_M), \phi_L'(\ell_1) = \phi_R'(\ell_1+\ell_M)\}$. Eqn (26) is then formulated in the context presented in Section II; however, these details are not included here due to space constraints.

B. Discretization

A basis $\{e_i\}_i^N$ is chosen for the approximating space $V^N \subseteq V$, where N corresponds to the number of basis functions used in the finite element approximation. Cubic Hermite interpolating polynomials are used to approximate the displacements of the left and right beams. The basis vectors take the form:

$$e_i^N = \begin{bmatrix} b_{L,i}^N(s_L) \\ b_{R,i}^N(s_R) \end{bmatrix},\ \text{for } i=1,\ldots,N. \tag{27}$$

That is, the state will be approximated as

$$\begin{bmatrix} w_L(t,s_L) \\ w_R(t,s_R) \end{bmatrix} \approx \begin{bmatrix} w_L^N(t,s_L) \\ w_R^N(t,s_R) \end{bmatrix} = \begin{bmatrix} \sum_{i=1}^N \alpha_i^N(t) b_{L,i}(s_L) \\ \sum_{i=1}^N \beta_i^N(t) b_{R,i}(s_R) \end{bmatrix}. \tag{28}$$

Substituting the state approximation (28) into (26) yields the matrix equation

$$\begin{aligned}
&M_L\ddot{\alpha}(t)+M_R\ddot{\beta}(t)+D_L\dot{\alpha}(t)+D_R\dot{\beta}(t)\\
&\quad+K_L\alpha(t)+K_R\beta(t)=B_Lu_L(t)+B_Ru_R(t)\\
&\qquad+G_L+G_R+F_L+F_R,
\end{aligned} \tag{29}$$

where

$$\begin{aligned}
[M_L]_{i,j} &= \int_0^{\ell_1}\rho A b_{L,i}(s_L)b_{L,j}(s_L)\ ds_L \\
&\quad +mb_{L,i}(\ell_1)b_{L,j}(\ell_1)+I_z b_{L,i}'(\ell_1)b_{L,j}'(\ell_1)\\
[M_R]_{i,j} &= \int_{\ell_1+\ell_M}^{\ell_1+\ell_M+\ell_2}\rho A b_{R,i}(s_R)b_{R,j}(s_R)\ ds_R\\
[D_L]_{i,j} &= \int_0^{\ell_1}\gamma_1 b_{L,i}(s_L)b_{L,j}(s_L)\ ds_L\\
&\quad +\int_0^{\ell_1}\gamma_2 I b_{L,i}''(s_L)b_{L,j}''(s_L)\ ds_L\\
[D_R]_{i,j} &= \int_{\ell_1+\ell_M}^{\ell_1+\ell_M+\ell_2}\gamma_1 b_{R,i}(s_R)b_{R,j}(s_R)\ ds_R\\
&\quad +\int_{\ell_1+\ell_M}^{\ell_1+\ell_M+\ell_2}\gamma_2 I b_{R,i}''(s_R)b_{R,j}''(s_R)\ ds_R\\
[K_L]_{i,j} &= \int_0^{\ell_1} EI b_{L,i}''(s_L)b_{L,j}''(s_L)\ ds_L\\
[K_R]_{i,j} &= \int_{\ell_1+\ell_M}^{\ell_1+\ell_M+\ell_2} EI b_{R,i}''(s_R)b_{R,j}''(s_R)\ ds_R\\
[B_L]_j &= \int_0^{\ell_1} b_L(s_L)u_L(t)b_{L,j}(s_L)\ ds_L\\
[B_R]_j &= \int_{\ell_1+\ell_M}^{\ell_1+\ell_M+\ell_2} b_R(s_R)u_R(t)b_{R,j}(s_R)\ ds_R\\
[G_L]_j &= \int_0^{\ell_1}\frac{m_b g}{\ell_1}b_{L,j}(s_L)\ ds_L\\
[G_R]_j &= \int_{\ell_1+\ell_M}^{\ell_1+\ell_M+\ell_2}\frac{m_b g}{\ell_2}b_{R,j}(s_R)\ ds_R\\
[F_L]_j &= \int_0^{\ell_1}-\frac{0.5\rho_a v^2 c}{\ell_1}C_\ell b_{L,j}(s_L)\ ds_L\\
[F_R]_j &= \int_{\ell_1+\ell_M}^{\ell_1+\ell_M+\ell_2}-\frac{0.5\rho_a v^2 c}{\ell_2}C_\ell b_{R,j}(s_R)\ ds_R,
\end{aligned} \tag{30}$$

which can be re-written as

$$\ddot{c}(t) = M^{-1}(-D\dot{c}(t)-Kc(t)+\bar{B}+\bar{G}+\bar{F}), \tag{31}$$

where

$$M = \begin{bmatrix} M_L & 0 \\ 0 & M_R \end{bmatrix}, \qquad D = \begin{bmatrix} D_L & 0 \\ 0 & D_R \end{bmatrix},$$

$$K = \begin{bmatrix} K_L & 0 \\ 0 & K_R \end{bmatrix}, \qquad \bar{B} = \begin{bmatrix} B_L \\ B_R \end{bmatrix}, \tag{32}$$

$$\bar{G} = \begin{bmatrix} G_L \\ G_R \end{bmatrix}, \qquad \bar{F} = \begin{bmatrix} F_L \\ F_R \end{bmatrix}.$$

Converting (31) into a first order system results in

$$\dot{x}(t) = Ax(t) + Bu(t) + G + F(x), \tag{33}$$

where

$$x(t) = \begin{bmatrix} c(t) \\ \dot{c}(t) \end{bmatrix}, \qquad A = \begin{bmatrix} 0 & I \\ -M^{-1}K & -M^{-1}D \end{bmatrix}$$

$$B = \begin{bmatrix} 0 \\ M^{-1}\bar{B} \end{bmatrix}, \qquad G = \begin{bmatrix} 0 \\ M^{-1}\bar{G} \end{bmatrix}, \tag{34}$$

$$F = \begin{bmatrix} 0 \\ M^{-1}\bar{F}(x) \end{bmatrix}.$$

Note that in this approximation of the BMB system, the A matrix sees free boundary conditions for displacement and slope at the free end of each beam, resulting in two zero eigenvalues for the system. While mathematically these free end conditions exist, physically, there are two external loads, lift and gravity, acting in equal and opposite directions across each beam. In some sense, these forces completely support the structure over the spatial domain. Consequently, it is necessary to communicate some existence of these external loads to the A matrix for control design. This is accomplished through a linearization of the original nonlinear PDE system.

V. NUMERICAL RESULTS

After linearizing (18) and (19), a Galerkin finite element approximation is obtained, and control design is implemented on the resulting system. The control objective is to morph each beam from equilibrium to the desired position

$$w(t,s) = \frac{5s(s-\ell)(2s-\ell)^2}{8w_{\text{peak}}}, \tag{35}$$

and slope

$$w'(t,s) = \frac{5(2s-\ell)(8s^2-8s\ell+\ell^2)}{8w_{\text{peak}}}, \tag{36}$$

where $w_{\text{peak}} = 0.0762$ m. The desired target shape is represented graphically in Figure 2, and is inspired from that which can be often seen in bird flight, for example.

To obtain a solution to the system of the form in (33), initial conditions are chosen as follows: $x(0) = [0;0;-2;0]$ (of the form [displacement; slope; velocity; angular velocity]). For the coupled state and state estimate system, the initial condition $x_c(0) = 0.75 * x(0)$ is used. It should also be noted that the balancing lift and gravity forces are modeled in the state estimate system as well. A convergent finite element approximation using Hermite interpolating cubic polynomials of order $N = 30$ nodes for the spatial discretization of the BMB system is used to simulate (33), and the parameter values for the BMB system are provided in Table I.

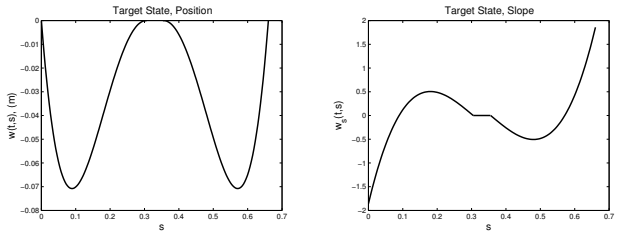

Fig. 2. Desired State Target: Position (left), Slope (right)

TABLE I
SYSTEM PARAMETERS

Parameter	Value	Units
$\ell_{1,2}$	0.6096	m
ℓ_M	0.0508	m
ρ	980	kg/m^3
$\hat{w}$, width	0.127	m
h, height	0.0254	m
$a = \hat{w}h$	0.032	m^2
E	2.0×10^6	N/m^2
$I = (\hat{w}h^3)/12$	1.734×10^{-7}	m^4
m	1.927	kg
m_b	1.927	kg
γ_1	0.025	kg/(m sec)
γ_2	1×10^2	kg/(m^5 sec)

For reference, the uncontrolled state plots for position and slope of the nonlinear system are given in Figure 3. Controlled results are presented in Figure 4, excluding noise. The corresponding controller plots are shown in Figure 5. To obtain stabilizing solutions to the algebraic Riccati equations, a Newton-Kleinman algorithm was used. For the results presented here, it is assumed that measurements are available for the position and slope states. Numerical instabilities in solving finite dimensional approximations to the algebraic Riccati equations occurred when it was assumed that only velocity and angular velocity were available for measurement. As expected, the full state feedback LQR results outperform those of the LQG-controlled system. Still, both controlled systems track well to the desired morphed wing shape. Simulations were also run for a traditional linear compensator with similar control and observation weights and forcing functions included. These results also showed good tracking, but with more initial overshoot, and are not presented here due to space constraints.

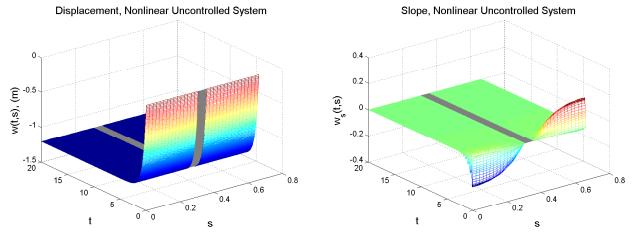

Fig. 3. Uncontrolled System: Position (left), Slope (right)

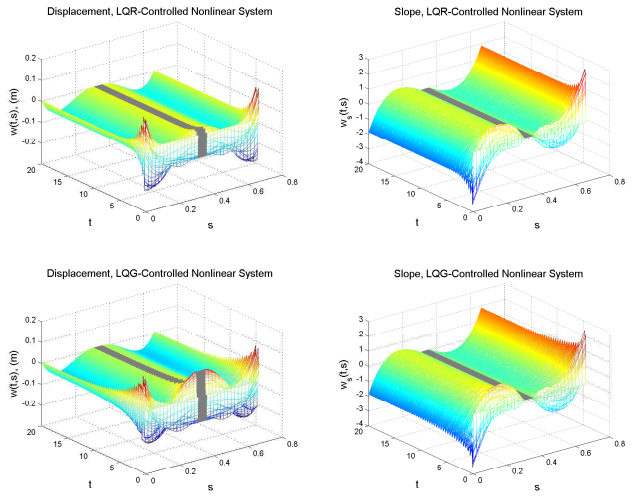

Fig. 4. Controlled System: LQR Position (top left), LQR Slope (top right), LQG Position (bottom left), LQG Slope (bottom right)

VI. CONCLUSIONS AND FUTURE WORKS

A. Conclusions

In this paper, the BMB system (18), (19), (21) is approximated by Hermite interpolating cubic polynomials with two displacement and two slope degrees of freedom for each beam element. Steady state linear quadratic tracking control was applied by obtaining a linear approximation of the nonlinear lift function, employing control design, and applying the control matrices to the nonlinear system. This resulted in a nonlinear controller for the BMB system.

B. Future Works

The authors are interested in applying realistic actuation and investigating optimal morphing trajectory for the BMB system. Consequently, analyzing the system's performance under various time-varying, morphing paths is of interest. The authors also seek to explore nonlinear control options to compare to the robustness of linear control techniques. Theoretical analysis results, including model well-posedness and semigroup analysis, are forthcoming.

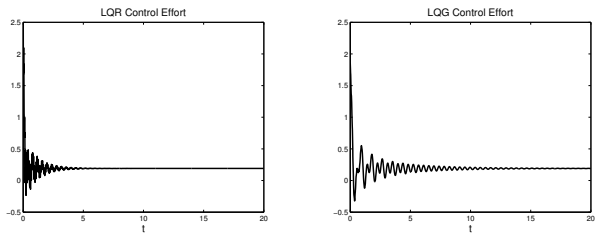

Fig. 5. Control Effort: LQG (left), LQR (right)

VII. ACKNOWLEDGMENTS

The authors gratefully acknowledge the contribution of the Louisiana Board of Regents, the US Air Force Summer Faculty Fellowship Program, the Air Force Research Laboratory and reviewers' comments. Portions of this research were conducted with high performance computational resources provided by the Louisiana Optical Network Initiative (http://www.loni.org/).

REFERENCES

[1] A. Chakravarthy, R. Albertani, N. Gans, and J. Evers, "Experimental kinematics and dynamics of butterflies in natural flight," *47th AIAA Aerospace Sciences Meeting Including The New Horizons Forum and Aerospace Exposition*, pp. AIAA–2009–873, 2009.

[2] W. Shyy, P. Ifju, and D. Viieru, "Membrane wing-based micro air vehicles," *Applied Mechanics Reviews*, vol. 58, pp. 283–301, 2005.

[3] W. Shyy, P. Trizila, C. Kang, and H. Aono, "Can tip vortices enhance lift of a flapping wing?" *AIAA Journal*, vol. 47, pp. 289–293, 2009.

[4] A. Song, X. Tian, E. Israeli, R. Galvao, K. Bishop, S. Swartz, and K. Breuer, "Aeromechanics of membrane wings, with implications for animal flight," *AIAA Journal*, vol. 46, no. 8, pp. 2096–2196, 2008.

[5] X. Tian, J. Iriarte-Diaz, K. Middleton, R. Galvao, E. Israeli, A. Roemer, A. Sullivan, A. Song, S. Swartz, and K. Breuer, "Direct measurements of the kinematics and dynamics of bat flight," *Bioinspiration & Biomimetics*, vol. 1, pp. S10–S18, 2006.

[6] R. Albertani, R. DeLoach, B. Stanford, J. Hubner, and P. Ifju, "Wind tunnel testing and nonlinear modeling applied to powered micro air vehicles with flexible wings," *AIAA Journal of Aircraft*, vol. 45, no. 3, 2008.

[7] R. Krashanitsa, D. Silin, S. Shkarayev, and G. Abate, "Flight dynamics of a flapping-wing air vehicle," *International Journal of Micro Air Vehicles*, vol. 1, pp. 35–49, 2009.

[8] A. Vargas, R. Mittal, and H. Dong, "A computational study of the aerodynamic performance of a dragonfly wing section ingliding flight," *Bioinspiration & Biomimetics*, 2008.

[9] L. Zheng, X. Wang, A. Khan, R. Vallance, R. Mittal, and T. Hedrick, "A combined experimental-numerical study of the role of wing flexibility in insect flight," *47th AIAA Aerospace Sciences Meeting Including The New Horizons Forum and Aerospace Exposition*, pp. AIAA–2009–382, 2009.

[10] J. S. Gibson, "An analysis of optimal model regulation: convergence and stability," *SIAM J. Contr. Opt.*, vol. 19, pp. 686–707, 1981.

[11] J. S. Gibson and A. Adamian, "Approximation theory for linear quadratic gaussian control of flexible structures," *SIAM J. Contr. Opt.*, vol. 29, pp. 1–37, 1991.

[12] P. Dorato, C. Abdallah, and V. Cerone, *Linear-Quadratic Control, An Introduction*. Englewood Cliffs: Prentice Hall, 1995.

[13] A. Chakravarthy, K. Evans, and J. Evers, "Sensitivities and functional gains for a flexible aircraft-inspired model," *Proceedings of the 2010 American Control Conference*, pp. 4893–4898, 2010.

[14] M. Dickinson, F. Lehmann, and S. Sane, "Wing rotation and the aerodynamic basis of insect flight," *Science*, pp. 1954–1960, June 1999.